Re-examining chemical conditions of past chamber studies of secondary organic aerosol formation

Matthew B. Goss,[1,2,3,*] Hannah S. Kenagy,[1,4] Colette L. Heald,[1,5] Jesse H. Kroll[1,6,*]

[1]Department of Civil and Environmental Engineering, Massachusetts Institute of Technology
[2]Harvard University Center for the Environment, Harvard University
[3]John A. Paulson School of Engineering and Applied Sciences, Harvard University
[4]Department of Chemistry, University of Minnesota
[5]Institute for Atmospheric and Climate Science, ETH Zürich
[6]Department of Chemical Engineering, Massachusetts Institute of Technology
*Corresponding authors

Abstract

The simulation of secondary organic aerosol (SOA) in 3D models generally relies on measurements made in laboratory chamber studies. However, many of the laboratory studies that underpin the aerosol parameterizations used in these models were carried out more than fifteen years ago, before recent developments in our understanding of peroxy radical (RO_2) chemistry and its role in aerosol formation. As a result, limitations of past chamber experiments and the incomplete understanding of their chemical conditions (e.g., the initiating oxidants, RO_2 fate), may skew SOA representation in models. In this work, literature SOA chamber studies, specifically those referenced by the SOA scheme in the GEOS-Chem global model, are simulated using a modified version of the Master Chemical Mechanism. This enables explicit estimation of typically-unconstrained parameters which affect experimental outcomes, including the relative importance of different oxidants, and the relative loss of RO_2 to different unimolecular and bimolecular processes. This work demonstrates that reaction conditions are dynamic, changing within and between experiments, and that many experimental conditions involve more than one oxidant or RO_2 fate, complicating model parameterizations. However, we also find that RO_2 isomerization is important under many of the experimental conditions used, meaning that some RO_2 isomerization processes are to some extent embedded into 3D model SOA estimates, despite no explicit representation of this chemistry.

Synopsis

We model past secondary organic aerosol chamber studies with explicit, detailed chemistry to explore the chemical conditions of the laboratory experiments that underpin aerosol parameterizations in 3D models.

Introduction

Secondary organic aerosol (SOA), formed from the oxidation and subsequent condensation of volatile organic compounds (VOCs), is the major component of organic aerosol in the atmosphere[1,2] and therefore substantially impacts the climate and contributes to air pollution. However, organic aerosol has long posed a challenge for 3D models, which typically do not accurately predict its observed variability,[3,4] likely due to the complexities and uncertainties associated with the formation of SOA.

SOA formation is strongly influenced by key branch points in the chemical oxidation mechanism, each of which operate as a function of reaction conditions.[5] Two of the most important branch points are the identity of the initiating oxidant and the fate of the resulting peroxy radical. VOCs are most commonly oxidized by OH, O_3, or NO_3, and these different oxidation pathways can affect SOA yield. For example, the reaction of isoprene with OH often results in relatively rapid incorporation of oxygen into the molecule, reducing volatility, while the reaction of isoprene with O_3 fragments the carbon chain, resulting in two oxidized but more volatile products. The oxidation of a VOC typically results in the formation of a peroxy radical (RO_2), a second key branch point that controls the distribution of potential products. Under a conventional understanding of RO_2 chemistry, RO_2 species typically react with NO, forming an alkoxy radical or organonitrate, or HO_2, forming an organic peroxide.[5] RO_2 species can also react with other RO_2, forming disproportionation or dimer products, and some RO_2 may react with NO_2, forming peroxyacyl nitrates, or with NO_3, forming alkoxy radicals.[6] These different RO_2 fates can affect SOA yields, for example by favoring fragmentation (yielding higher volatility products) or incorporation of additional oxygen atoms (yielding lower volatility products).

However, advances in our understanding of RO_2 chemistry over the last fifteen years have brought to light several new RO_2 reaction pathways. In particular, peroxy radical isomerization, sometimes referred to as autoxidation, has been recognized as an important pathway through which oxygen may sequentially be incorporated into an organic molecule, rapidly forming a low-volatility compound that may condense to efficiently contribute to SOA mass.[7,8] RO_2 isomerization rates are highly dependent on the structure of the RO_2 species, varying over many orders of magnitude, such that for some compounds, it may be a dominant RO_2 fate, while for others it may be irrelevant.[9] While additional RO_2 reactions such as the rapid formation of ROOR species by $RO_2 + RO_2$[10] or the reaction of RO_2 with OH[11] have also been discovered in recent years, the importance of these for atmospheric SOA formation is not yet clear.

The formation of SOA is sufficiently complex such that its explicit modeling on a regional and global scale is prohibitive. SOA forms through the condensation of numerous products of VOC oxidation, each of which is derived from a different complicated (and incompletely understood) sequence of oxidation reactions, and each of which differ in vapor pressure and reactivity. In order to make this process computationally tractable, 3D models rely on substantial simplifications. In the simplest case, SOA is treated as a fixed yield product of the reaction or

emission of VOC precursors.[3,12] However, SOA is more realistically represented when absorptive partitioning of gas-phase organic species into the organic aerosol phase is considered,[13] typically through the use of the two-product model[14] or volatility basis set (VBS).[15] In either case, yields of surrogate species of different volatilities are assigned by fitting the laboratory-measured SOA yield as a function of the organic aerosol concentration (c_{OA}), thereby linking laboratory results to 3D model output. While SOA yields in a VBS scheme can be defined simply based on the identity of the VOC precursor, they may also be specified based on VOC/oxidant pairs, or NO_X-conditions ("high NO_X" and "low NO_X"), such that aerosol yields in the model can be defined for different chemical environments. Within this framework, aerosol yields may be parameterized such that under intermediate chemical conditions (e.g., competing RO_2 + NO and RO_2 + HO_2 reactions), SOA yields may be linearly interpolated.[16–18]

Because SOA parameterizations fundamentally rely on laboratory chamber experiments, they therefore integrate any limitations from these experiments. Many limitations of chamber experiments have been documented previously, including large differences between atmospheric and chamber temperature, humidity, and NO_X concentrations,[19] as well as the partitioning of semi-volatile and low-volatility species to chamber walls, a process which impacts observed aerosol formation.[20] An important additional limitation is that the chemical conditions used in past chamber experiments are not typically well-characterized.[21] Many laboratory chamber studies that continue to be used as a basis for regional and global model aerosol modules were carried out more than fifteen years ago, before the previously-discussed advances in our understanding of RO_2 chemistry (e.g., isomerization). Earlier chamber experiments were not designed to study these unimolecular reaction pathways, and instead focused on separating aerosol yield by reaction with specific oxidants, and/or by "high-NOx" vs "low-NO_X" pathways. Furthermore, while assessments of RO_2 and oxidant fate in contemporary chamber experiments using mechanistic modeling is increasingly common, it was much less common in older studies. Instead, oxidant and RO_2 fate was often assumed based on the oxidant added or the initial NO_X concentrations, and any such assumptions are subsequently embedded in aerosol parameterizations. While contemporary model schemes rely on a range of laboratory studies, they often pull from some of the same older experiments; commonly referenced collections of volatility basis set fits include Pye et al.,[18] Farina et al.,[12] and Zhang et al.[22]

Given our evolving understanding of radical chemistry, the chemical conditions as reported in older publications and the chemical conditions actually used in those experiments may not always align. Where an aerosol parameterization relies on assigned RO_2 conditions (e.g., reaction with NO vs. reaction with HO_2), any deviation in the true experimental RO_2 fate from this binary classification (which may arise from the importance of other reactions such as isomerization or RO_2 + RO_2) may affect the accuracy of the aerosol scheme. Similarly, oxidation processes may differ from an assumption of a single dominant oxidant, as multiple oxidants may be formed (e.g., OH from O_3 + alkene reactions, O_3 or NO_3 from irradiated VOC + NO_X mixtures). These effects may be unexpected, for example where these processes are influenced by trace background NO_X or by the chemistry associated with added compounds (e.g., OH scavengers).

This work seeks to re-examine chamber conditions used in literature SOA experiments, by using explicit box modeling to estimate typically-unconstrained chemical parameters. The specific focus here is on the initiating oxidant and the fate of RO_2 radicals, which to our knowledge have never been systematically assessed in past SOA chamber studies. The set of historical chamber experiments examined is taken from the basis for the "Complex" aerosol scheme[18] from GEOS-Chem, a widely used chemical transport model. This scheme describes SOA formation in terms of both oxidant and RO_2 fate, and therefore represents an appropriate study to use as a guide for the selection of experiments. While this set of experiments is not a comprehensive list, it includes chamber studies that form a basis for aerosol schemes in other 3D models, such that the results of this work may be more broadly applicable. Chamber experiments are represented using explicit chemical mechanisms, modified where possible to include appropriate isomerization reactions. Finally, explicitly modeled oxidant and RO_2 fate are interpreted in the context of their use in aerosol parameterizations, giving insight into challenges facing experimental design and the creation of accurate parameterizations.

Methods

Historical experiments are chosen based on Pye et al.,[18] the basis for the "Complex" aerosol scheme used in GEOS-Chem. While subsequent studies have updated the aerosol module to include aqueous reactive uptake of isoprene oxidation products and some organonitrates separately from the volatility basis set,[23,24] that work is not considered here. The publications covered in this work are shown in Table 1, along with basic experimental details and a brief summary of data availability. Starting experimental conditions (NO_X levels, VOC levels, etc.) are provided in each publication, and experimental timeseries are scraped from paper figures or provided by authors. All model parameters for each simulation are shown in Tables S.1 and S.2.

Each experiment is classified into one of six categories (last column of Table 1) based on the oxidation conditions. While chamber experiments are often grouped simply as "high-NO_X" or "low-NO_X," these distinctions do not fully describe the underlying chemistry or RO_2 fate.[25] Experiment categories involving added NO_X include "HONO" (which use HONO as an oxidant precursor[26,27]), "H_2O_2, NO_X" (which use both H_2O_2 and added NO_X[26,28]), and "traditional photooxidation" (which use a mixture of VOC, NO_X, and UV light[29]). Experiments using VOC, NO_X, UV light, and added O_3[30] are also grouped into this category based on similarities in the observed chemistry. Experiment categories involving no added NO_X include "H_2O_2, low NO_X," [28,27,26] and "O_3, low NO_X".[29,31] In all ozonolysis experiments studied here, an OH scavenger is added to minimize OH oxidation of the precursor. Ozonolysis experiments from Zhang et al.[30] are classified as "O_3, some NO_X" since these experiments featured measurable background NO_X concentrations of 2 – 15 ppb (sufficiently high to substantially alter observed chemistry).

Table 1: Summary of modeled experiments.[a]

Publication	VOC Precursors	Number of expts.	Reference data	Oxidation category
Griffin et al.[29]	β-pinene β-caryophyllene α-pinene	5	Starting conditions (all expts) + time series (one expt)	O_3, low NO_X Traditional photooxidation
Zhang et al.[30]	limonene	22	Starting conditions (all expts) + time series (two expts)	O_3, some NO_X Traditional photooxidation
Kroll et al.[28]	isoprene	14	Starting conditions (all expts) + max. O_3 concentrations (all expts) + time series (two expts)	H_2O_2, low NO_X H_2O_2, NO_X
Ng et al.[27]	*m*-xylene toluene benzene	18	VOC, NO_X, O_3 time series (all expts)	H_2O_2, low NO_X HONO
Ng et al.[26]	α-pinene	5	VOC, NO_X, O_3 time series (all expts)	H_2O_2, low NO_X H_2O_2, NO_X HONO
Shilling et al.[31]	α-pinene	8	Starting conditions (all expts)	O_3, low NO_X

[a]Model parameters for each experiment are included in Tables S.1 and S.2.

Modeling is carried out using the Framework for 0-D Atmospheric Modeling, version 4.3 (F0AM).[32] Chemical mechanisms are taken from the Master Chemical Mechanism (MCM v3.3.1).[33,34,34–37] While referenced by Pye et al.,[18] α-humulene and naphthalene are not modeled since they are not represented in the MCM. Similarly, experiments focusing on the reaction of NO_3 with β-pinene[29] and isoprene[38] are also omitted due to insufficient experimental data to constrain the model. Only gas-phase chemistry is modeled, with no treatment of partitioning or particle-phase chemistry.

While some mechanisms in the MCM, most notably for isoprene, include unimolecular RO_2 reactions, most mechanisms used here do not yet feature unimolecular RO_2 chemistry. While RO_2 isomerization rates are highly dependent on structure[9] and challenging to accurately measure or calculate, some important isomerization rates have been characterized or estimated for all of the precursor VOCs studied. Mechanisms are therefore modified to include known or estimated RO_2 isomerization rate constants for initial RO_2, defined here as the first RO_2 species formed immediately after the VOC-oxidant reaction (these species are listed in Table S.3); all other RO_2 are referred to as "subsequent" RO_2. We note that because a single generation of oxidation can include multiple RO_2 species formed in sequence, "initial RO_2" is not synonymous with "first-generation RO_2." Due to the extensive uncertainties and complexities of integrating unimolecular RO_2 reactions into chemistry that occurs beyond the initial RO_2 species, reactions for subsequent RO_2 are not modified. To conserve carbon without extensively re-writing each mechanism, each RO_2 isomerization reaction forms an alkyl radical, which reacts with oxygen to form another RO_2 radical, identical to an RO_2 species from a later point in the mechanism. RO_2 isomerization rate constants are taken from literature measurements and calculations.[9,39–44]

Mechanism modifications are applied to all precursor mechanisms (except that of isoprene, which already features isomerization reactions), and are detailed in Table S.4 and Section S.1.

Some experiments use additional VOCs such as radical promoters (propene),[29] which facilitate additional OH formation through ozonolysis, OH scavengers (2-butanol, *n*-butanol),[29–31] which decrease OH concentrations to maximize O_3 chemistry, or hydrocarbons (*n*-pentane),[30] which are used to dilute the precursor VOC for injection. These species are represented by a standard mechanism from the MCM and an identical non-interacting tracer mechanism that is run in parallel with the main simulation. This allows the subtraction of the influence of these species during analysis, such that analysis focuses solely on the chemistry of the VOC of interest.

All experiments are first modeled based on known parameters. While the publications vary in specificity with regard to reported conditions, they generally report initial VOC, O_3, and NO_X concentrations (See Tables S.1 and S.2 for a summary of all model input parameters). Less well quantified starting material concentrations include H_2O_2 (typically estimated) and OH radical sinks (e.g. 2-butanol concentration is "sufficient to consume OH" [29]). Light spectra are taken from earlier publications for indoor chambers[45,46] (See Figure S.1). Experiment length is rarely stated explicitly and is assumed to be the same as the length of time shown in relevant figures, or the length of time in relevant data files. Since the experiments simulated do not quantify vapor wall losses, these processes are not represented in the model.

For each series of experiments, model runs are then tuned to match measured data by adjusting free variables that are unmeasured or poorly quantified. Chamber light intensity is adjusted to match reported j_{NO2} values[28] or to fit reported VOC, NO_X, and O_3 timeseries.[29,30] For the outdoor experiments of Griffin et al.,[29] the default sunlight intensity based on experimental date and location is halved to best match data, likely a result of overhead aerosol or clouds. For experiments using HONO as an oxidant precursor, a combination of NO_X analyzer measurements (which measure HONO as "NO_2"), and fit to measured timeseries of VOC, NO_X, and O_3 are used to constrain HONO concentrations. H_2O_2 concentrations are unmeasured but estimated in several publications. While these are generally taken as the mean value of the estimated range, the concentration is loosely constrained by the NO loss rate (which is sensitive to H_2O_2 concentrations) when NO is present in the experiment. For several experiments with no added NO_X, ozone is produced when little is predicted; this is likely due to residual NO_X species off-gassing from the chamber walls.[28] In these cases, ozone timeseries are best matched by adding trace NO or NO_2 to the model; in some cases, this is held constant (see Table S.2). Even when ozone formation does not constrain [NO_X], experimental conditions are unlikely to be truly NO_X-free, so a small amount of NO_2 (0.1 – 1 ppb, below reported detection limit) is added to the model. For variables that are not quantitatively constrained (e.g., a reported j_{NO2} value), final tuning of these input parameters is carried out by eye to achieve a reasonable fit to reported VOC, NO_X, and O_3 timeseries.

Since some experimental parameters are relatively uncertain, the effect of variability in model inputs is explored through sensitivity testing. Light intensity and all nonzero starting

concentrations are varied individually by ± 30%. These results are first used to assess how uncertainty in starting conditions impacts the fit between measurement and modeled results. As described in Results and Discussion, these sensitivities are also used to explore how uncertainty in starting conditions propagates to measured parameters associated with subsequent chamber chemistry.

Relative VOC reactive loss pathways and RO_2 fates are calculated based on F0AM outputs, which include time series of all species in the mechanism and rates over time for each reaction. Reactive loss pathways include reaction with OH, O_3, or NO_3, as well as direct photolysis for photolabile product species such as formaldehyde. We extract reaction rates for each "oxidant" (including *hv*) over time and separate them into reactions with the precursor and reactions with other organic products. These time series are interpolated, summed, and normalized to get total fractional reactive loss pathways for both precursor and total products. Peroxy radical fate is assessed in a similar way. Peroxy radicals are grouped into initial RO_2 and subsequent RO_2, and time-dependent RO_2 reaction rates ($RO_2 + HO_2$, $RO_2 + NO$, $RO_2 + NO_2$, $RO_2 + RO_2$, $RO_2 + NO_3$, unimolecular RO_2 reaction) are then extracted from the model output. In order to properly account for the relative importance of reversible RO_2 reactions, most notably acyl $RO_2 + NO_2$ reactions which generate peroxyacyl nitrates (PANs), rates are calculated by summing any equilibria such that the reported rate is equal to the net flux (using the F0AM function ExtractRates with the "sumEq" parameter set to 1). This does not affect calculated rates for other RO_2 reactions, which are not reversible in the MCM. As above, grouped RO_2 fate timeseries are used to obtain total fractional RO_2 fate for initial and subsequent RO_2. For all model outputs, the influence of radical promoters, OH scavengers, and additional hydrocarbons is removed using the output of the tracer mechanism.

Model outputs are further interpreted with respect to the fraction of RO_2 reacting with NO vs HO_2, β, and the bimolecular peroxy radical lifetime, τ_{bi}. As defined in Pye et al.[18], β enables assessment of the competition between reaction with HO_2 and NO (eq. 1), and is used as a "mixing parameter" in SOA parameterizations to interpolate aerosol yields measured under "high-NO" and "low-NO" conditions.[16–18]

$$\beta = \frac{k_{RO_2+NO}[NO]}{k_{RO_2+NO}[NO] + k_{RO_2+HO_2}[HO_2]} \quad (1)$$

The bimolecular peroxy radical lifetime,[47–49] τ_{bi}, can be used to assess the relative importance of unimolecular RO_2 chemistry. Since unimolecular RO_2 reaction rates vary over many orders of magnitude, τ_{bi} can be used as a threshold to indicate whether a given unimolecular reaction would be competitive, relative to the unimolecular lifetime, τ_{uni} (the inverse of the unimolecular RO_2 reaction rate constant). While prior work has often defined τ_{bi} only with respect to bimolecular reaction with NO and HO_2,[49,21] we define τ_{bi} with respect to reaction with NO, HO_2, RO_2, NO_2, and NO_3 (eq. 2), since under some chamber conditions, these additional reactive sinks are found to contribute to RO_2 loss.

$$\tau_{bi} = \frac{1}{k_{RO_2+NO}[NO] + k_{RO_2+HO_2}[HO_2] + k_{RO_2+RO_2}[RO_2] + k_{RO_2+NO_2}[NO_2] + k_{RO_2+NO_3}[NO_3]} \quad (2)$$

The bimolecular lifetime is calculated using rates extracted from the model, and does not take into account substantially faster recent measurements of the RO_2 + RO_2 rate constants.[10]

Results and Discussion

Model-measurement agreement and example model output

Figure 1A shows an example model-measurement comparison from a "traditional photooxidation" experiment in which β-pinene was oxidized in the presence of NO_X, propene, and sunlight.[29] The model agrees qualitatively with the measurements, and nearly all values fall within the envelope of timeseries generated by the sensitivity testing (lightly shaded areas). While modeled NO_2 diverges from the measurements late in the experiment, this might not be a model error, and instead could be a result of NOy species (e.g., PANs, organonitrates) reported as NO_2 by commercial NO_X monitors. For most experiments, measurements similarly qualitatively agree with model estimates (Figures S.2 and S.3).

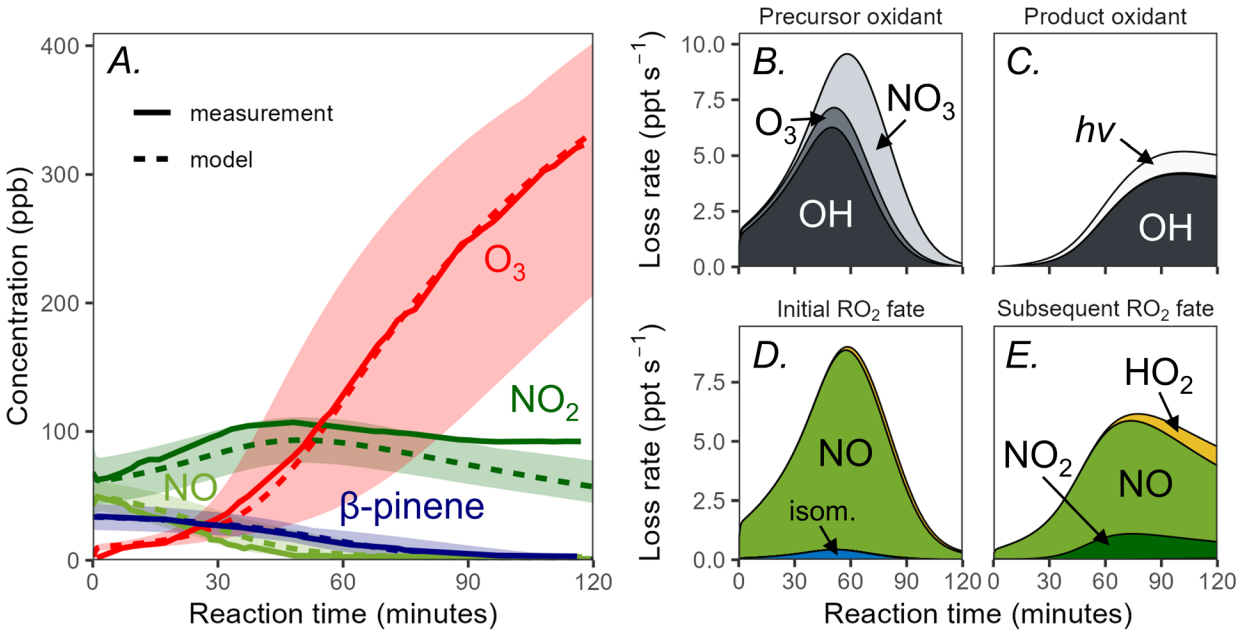

Figure 1: Model-measurement comparison from an example experiment (Panel A), and stacked time series of oxidant and RO_2 loss rates (panels B – E). The experiment shown is a traditional photooxidation experiment in which β-pinene is oxidized in the presence of NO_X and propene (expt. #1, see Table S.1).[29] Panel A shows both modeled and measured time series for four species, with shaded regions representing the upper and lower bounds based on sensitivity testing. Panels B – E separate precursor from product loss pathways, and separate initial and subsequent RO_2 fate.

However, the tuned model deviates from measurements in several experiments, most notably for H_2O_2 + NO_X experiments,[26,28] in which measured O_3 is well below the model value. The cause of

this is unclear, and is not resolved by modulating light intensity or H_2O_2 concentrations. To explore the impact of this difference, modeled O_3 concentrations are fixed to measured values and model outputs are recalculated for one experiment for which this occurs. These differ little from those derived from the original model run (see Figure S.4).

Figure 1B-E shows oxidation rates and RO_2 fate over time for the example experiment. The precursor β-pinene reacts mostly with OH, but NO_3 becomes an important oxidant as the experiment proceeds (Figure 1B). Organic products also react mostly with OH, but photolysis increases in relative importance as formaldehyde and other photolabile aldehydes are formed (Figure 1C). Similarly, RO_2 fate differs for initial vs subsequent RO_2. Initial RO_2 reacts mainly with NO, with a small contribution from isomerization (Figure 1D). While NO is still the main contributor to subsequent RO_2 fate, $RO_2 + HO_2$ and acyl $RO_2 + NO_2$ reactions become increasingly important later in the experiment (Figure 1E). This demonstrates how oxidant and RO_2 fate can evolve substantially over the course of a given experiment.

Relative VOC reactive losses

Integrated VOC reactive loss pathways for a larger selection of experiments are presented in Figure 2. This figure shows fractional loss rates to each oxidant for the precursor VOC (first column) and the organic products (second column) for a selection of experiments. These experiments are chosen to represent a range of precursors and oxidation categories, illustrating the variety of oxidant fates seen across the experiments modeled in this study.

In these experiments, researchers generally sought to achieve chemical conditions in which one oxidant was dominant, for example by using an OH scavenger in ozonolysis experiments to encourage O_3 chemistry to dominate. This is largely achieved for several experiment types—HONO, $H_2O_2 + NO_X$, low-NO_X H_2O_2, and low-NO_X ozonolysis all feature precursor oxidation largely driven by a single oxidant (OH or O_3). However, this is not the case for traditional photooxidation experiments, or the "O_3, some NO_X" experiments. These experiments feature a mix of oxidants, in which oxidation by NO_3 competes with oxidation by OH and O_3.

The distribution of reactive pathways for reaction products (second column of Figure 2) is dramatically different from that for precursors. Ozone reactivity is decreased as double bonds are consumed, and photolysis becomes an important loss pathway, since many products include photolabile functional groups. A majority of this photolysis is of small aldehydes (e.g., formaldehyde, glyoxal), but larger species can also contribute, depending on the VOC precursor. While changing reactivity explains many of the differences between fractional loss of the precursor and the products, these differences are also affected by temporal shifts in oxidant concentrations across an experiment (e.g., increasing O_3 levels).

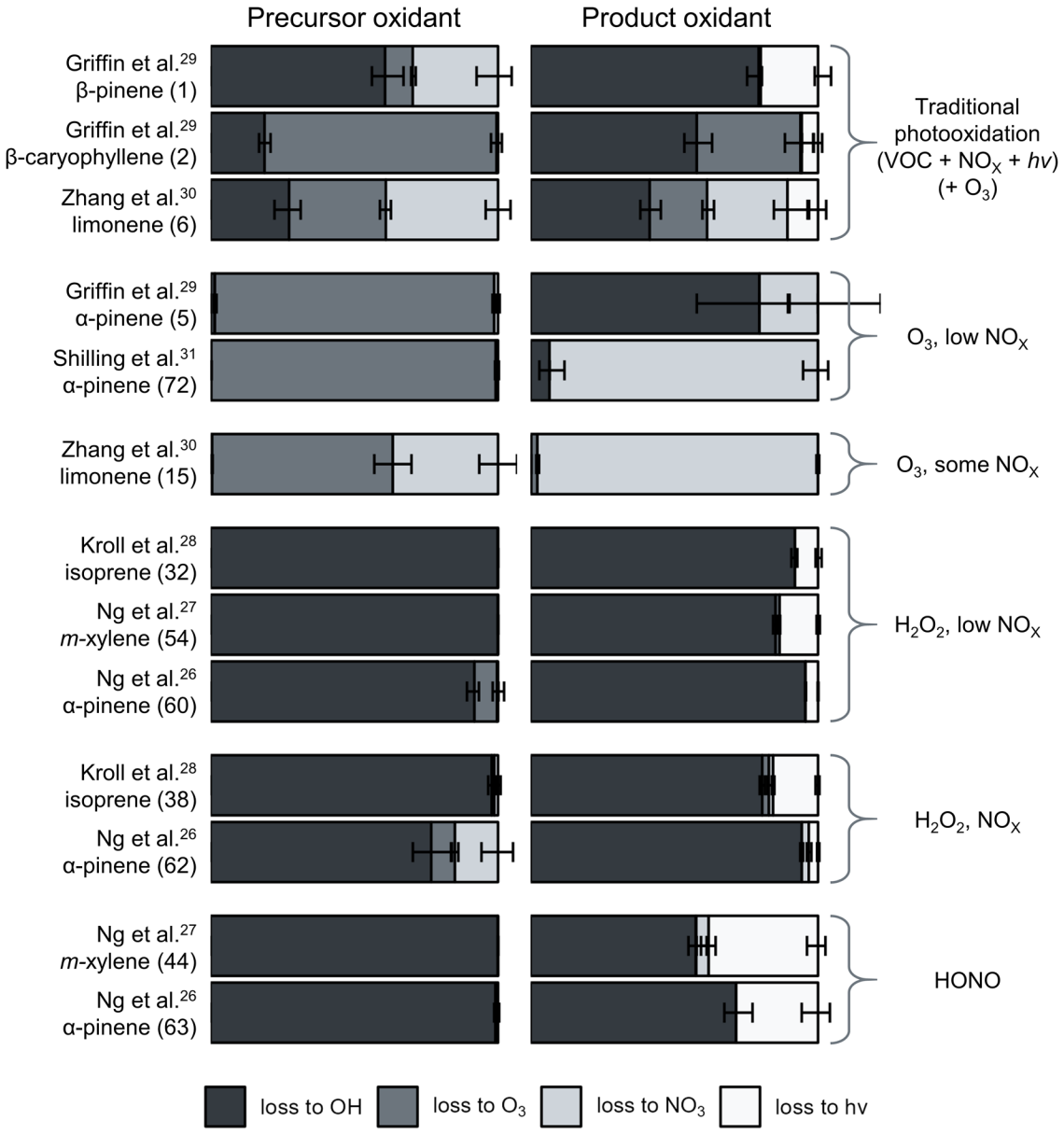

Figure 2: Fractional precursor and product loss by different oxidants. Precursor losses are shown in the left column, and product losses are shown in the right column. Experiments are grouped by experimental conditions, and selected such that each represents a distinct set of starting conditions. Experiment numbers are found in parentheses following the VOC names (see Table S.1). Error bars reflect the range of values observed in response to sensitivity tests and represent the range for each oxidant, not the cumulative range. Error bars do not reflect any uncertainties propagated from errors or uncertainties in the chemical mechanisms.

Figure 2 also shows error bars representing the range of values observed across sensitivity tests. Despite varying model inputs by 30%, the ranges observed here are far lower in most cases, indicating that these results are relatively robust to uncertainties in experimental starting conditions. The main exception is uncertainties driven by trace NO_2 added to low-NO_X ozonolysis experiments (since none of these experiments are carried out under perfectly NO_X-

free conditions). Perturbations to trace NO_2, e.g., in α-pinene oxidation carried out by Griffin et al.,[29] substantially affect the fraction of oxidation products lost to reaction with NO_3, resulting in larger error bars. This effect is similarly observed for Shilling et al.[31] where relatively little total product oxidation occurs, leaving later oxidation dominated by NO_3 reactions (since NO_3 is not consumed by reaction with the OH scavenger *n*-butanol in the MCM). We note that the uncertainty ranges shown here do not include possible uncertainties in the chemical mechanism, which may be substantial but are beyond the scope of this work.

RO_2 fate

Figure 3 shows modeled RO_2 fate for the same set of experiments as shown in Figure 2. This figure shows total fractional RO_2 fate separated between initial and subsequent RO_2, grouped again by experiment type.

Most OH experiments (with the exception of the traditional photooxidation experiments) feature conditions designed to favor one RO_2 fate. For experiments in which researchers sought to force all RO_2 through reaction with NO (e.g. "HONO" and "H_2O_2, NO_X" experiments), this is often achieved for initial RO_2. Likewise, reactions with high concentrations of H_2O_2 but no added NO_X typically involve reaction with HO_2 as a majority of initial RO_2 fate (e.g. Kroll et al. low-NO_X oxidation of isoprene[28]).

However, numerous experiments feature mixed RO_2 fates, particularly with regard to the influence of RO_2 isomerization. RO_2 isomerization represents an important initial RO_2 reaction channel, particularly for the "low-NO_X ozonolysis" experiments,[29,31] but also for the "low-NOx H_2O_2" experiments[26,28] and even for some experiments in which NO_X was added.[27,29,30] In many cases, the isomerization rates are fast enough to dominate the chemistry of a given RO_2, outcompeting bimolecular reaction, but limited by the fact that only some RO_2 can undergo isomerization. In the extreme example of this, ring closure reactions for aromatic species are considered fast enough ($\tau_{uni} < \sim 10^{-4}$ s)[42] to outcompete bimolecular reaction under all conditions (for this reason, the only bimolecular reactions for initial RO_2 from *m*-xylene (Fig. 3) stem from the minor OH reaction channel). For RO_2 isomerization reactions that involve H-atom abstraction and hence have slower isomerization rates (e.g., $\tau_{uni} = 0.25$ s^{-1} for one α-pinene-derived RO_2[44]), reaction conditions can substantially affect the degree of isomerization. For example, the importance of isomerization in the oxidation of α-pinene by Ng et al.[26] shifts considerably between experiments with and without added NO_X (Figure 3). While the concentrations of HO_2 and NO required to largely shut off the isomerization pathway vary with the isomerization rate, Figure 3 suggests that HO_2 concentrations for H_2O_2 experiments are typically not high enough to fully suppress unimolecular chemistry. This agrees with previous work showing that isomerization (assuming a rate constant of ≥ 0.1 s^{-1}) is only partially suppressed even when [H_2O_2] is as high as 10 ppm.[50] In contrast, reaction with NO can fully suppress these pathways, but only when large excesses of NO are added (e.g., hundreds of ppb NO in the oxidation of α-pinene with HONO[26]).

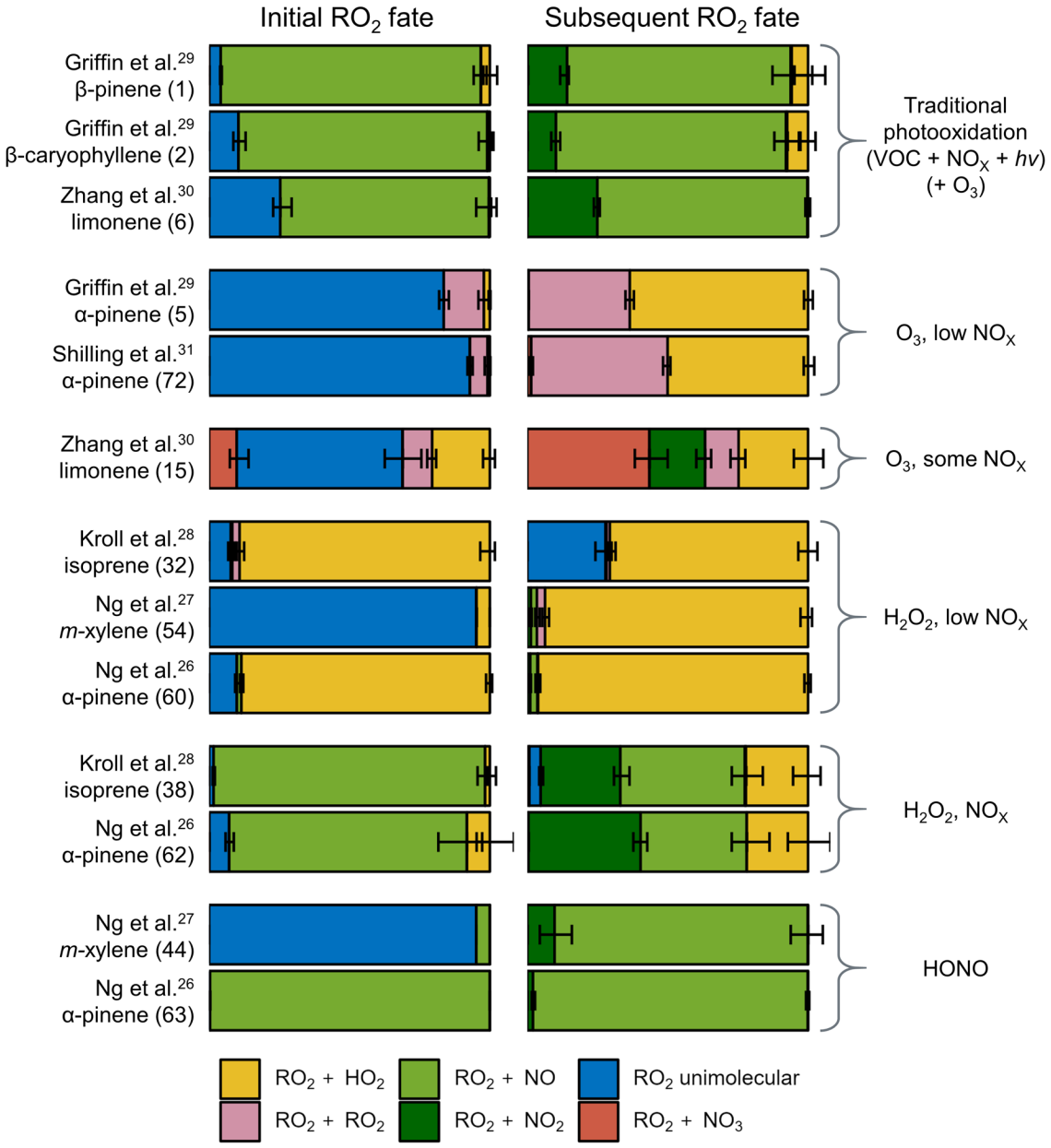

Figure 3: Fractional RO_2 loss rates, grouped by initial RO_2 (left column) and subsequent RO_2 (right column) for selected experiments (same as shown in Figure 2). As in Figure 2, error bars reflect the range of values observed in response to sensitivity tests and represent the range for each type of reaction, not the cumulative range; they do not reflect any uncertainties propagated from errors in the chemical mechanisms.

Subsequent RO_2 chemistry can be dramatically different than that of the initial RO_2. While this is impacted by a lack of isomerization reactions in the reaction mechanisms (see Methods), bimolecular pathways also shift substantially, due to changing reactivity and changing reactant concentrations. One clear change is the increase in reaction with NO_2, driven by increased NO_2/NO ratios (Figure 1) and formation of acyl peroxy radicals, leading to increased $RO_2 + NO_2$ reactions forming PAN. $RO_2 + RO_2$ reactions notably also increase for "low-NO_X ozonolysis

experiments," where RO_2 concentrations are enhanced by the products of OH reaction with added OH scavengers, and NO and HO_2 concentrations remain relatively low. Finally, in the case of isoprene, for which the MCM includes several unimolecular reactions of subsequent RO_2, isomerization increases in relative importance, in part to due to the gradual increases in τ_{bi} that occur throughout some experiments. While much of this subsequent isomerization is of RO_2 species formed directly from the initial RO_2 isomerization, it also includes substantial contributions from the oxidation of first-generation reaction products (e.g., OH + isoprene epoxydiol and OH + methacrolein).

Like in Figure 2, the range of RO_2 fates simulated with perturbed starting conditions (error bars in Figure 3) is smaller than the range of perturbations, suggesting these values are relatively robust to error in initial conditions. Imperfections in the chemical mechanisms, perhaps most notably the lack of later-generation RO_2 isomerization reactions likely contribute a larger (but unknown) error to RO_2 fate.

Comparison with SOA parameterizations

Chemical conditions as modeled here can be compared to how these experiments are used in the GEOS-Chem aerosol parameterization. As mentioned above, the "Complex" aerosol scheme in GEOS-Chem specifies aerosol yield parameters as a function of β, the fraction of RO_2 reacting with NO instead of HO_2. Table 2 presents the classification of experiments used for GEOS-Chem[18] alongside modeled oxidant and RO_2 chemistry parameters.

In most cases, RO_2 fates calculated here and those assumed in the parameterization generally agree. This is particularly evident where conditions are pushed to very high levels of NO or HO_2 and β falls near 1 or 0.[27,28] However, several differences stand out. Sesquiterpene oxidation experiments from Griffin et al.[29] feature a mean β value of 0.93, indicating NO as a dominant RO_2 fate, but are used for parameterizing SOA at low-β (RO_2 + HO_2) conditions. While β values from Zhang et al.[30] (limonene) and Shilling et al.[31] ("monoterpenes") experiments fall near expected extremes, β may not appropriately characterize these experiments due to the importance of other RO_2 pathways. A large fraction of the overall bimolecular RO_2 fate (Table 2) does not involve NO or HO_2 in these sets of experiments, indicating that these experiments may not serve as an ideal basis for SOA parameterizations relying on β.

Table 2: Comparison between GEOS-Chem aerosol parameterization conditions and results from this work.[a]

GEOS-Chem				This work			
Parent hydrocarbon	Citation	Assumed RO_2 fate	Assumed oxidant	Expt. #	Mean β (1σ)	Mean bimolecular RO_2 fate (HO_2 % / NO % / other %)	Mean precursor oxidant fraction (OH % / O_3 % / NO_3 %)
Limonene	30	NO	OH, O_3	16 – 27	0.88 (0.14)	2 / 23 / 75	1 / 27 / 73
Monoterpenes[b]	c	NO	OH, O_3	-	-	-	-
Sesquiterpenes[b]	d	NO	OH, O_3	-	-	-	-
Limonene	30	HO_2	OH, O_3	8 – 15	0 (0)	13 / 0 / 87	2 / 74 / 24
Monoterpenes[b]	31	HO_2	OH, O_3	65 – 72	0 (0)	25 / 0 / 75	0 / 97 / 3
Sesquiterpenes[b]	29	HO_2	OH, O_3	2 – 4	0.93 (0.04)	6 / 86 / 8	19 / 81 / 0
Isoprene	28	-	OH	28 – 35	0 (0)	98 / 0 / 1	100 / 0 / 0
Benzene	27	NO	OH	50	1 (-)	0 / 95 / 4	100 / 0 / 0
Toluene	27	NO	OH	46 – 49	1 (0)	0 / 99 / 1	100 / 0 / 0
Xylene	27	NO	OH	42 – 45	1 (0)	0 / 97 / 3	100 / 0 / 0
Benzene	27	HO_2	OH	59	0.04 (-)	92 / 4 / 4	100 / 0 / 0
Toluene	27	HO_2	OH	55 – 58	0.01 (0)	95 / 1 / 3	100 / 0 / 0
Xylene	27	HO_2	OH	51 – 54	0.02 (0.01)	95 / 2 / 3	100 / 0 / 0

[a] This table is based on Table 1 from Pye et al.,[18] omitting rows that do not correspond to model runs in this study. Values correspond to modeled oxidant and RO_2 chemistry from experiments used to generate the VBS parameterization. Note that the total mean bimolecular RO_2 fate does not include isomerization reactions. Standard deviations reflect the variation within the set of experiments.

[b] Monoterpene parameterization is based on α-pinene. Sesquiterpene parameterization is based on β-caryophyllene and α-humulene, but only β-caryophyllene model data is used here since α-humulene is not in the MCM.

[c] In Pye et al.,[18] corresponding low-NO_X monoterpene data[31] is scaled by a factor of 0.5 based on Ng et al.[26] and Pathak et al.[51] There are therefore no direct model runs that correspond to this parameterization.

[d] In Pye et al.,[18] corresponding "low-NO_X" sesquiterpene data[29] is scaled by a factor of 2 based on Ng et al.[26] There are therefore no direct model runs that correspond to this parameterization.

Similarly, Table 2 illustrates that most experiments feature precursor oxidation by OH or O_3, consistent with assumptions in the aerosol parameterization. The most notable exception to this however is the oxidation of limonene in high-NO_X experiments,[30] where ~73% of the precursor is oxidized by NO_3. These experiments may be better suited to a parameterization of SOA formation following reaction with NO_3, since the formation of organonitrate species may impact aerosol yields[52] relative to reaction only with OH and O_3.

Perhaps the most important difference between the SOA parameterization[18] and the box modeling results (Figure 3) is that β-based parameterizations do not explicitly capture isomerization. The potential importance of RO_2 isomerization can be described in terms of the RO_2 bimolecular lifetime, τ_{bi}.[47,49] This metric enables comparison of RO_2 conditions in chamber experiments to atmospheric conditions,[21] in addition to facilitating the interpretation of trends in

RO_2 isomerization. Figure 4 shows the bimolecular lifetime for each experiment considered in this study, in comparison with the global distribution of bimolecular lifetimes (weighted by the isoprene oxidation rate) taken from GEOS-Chem (version 13.4.0, from hourly output for January and July 2016).[21]

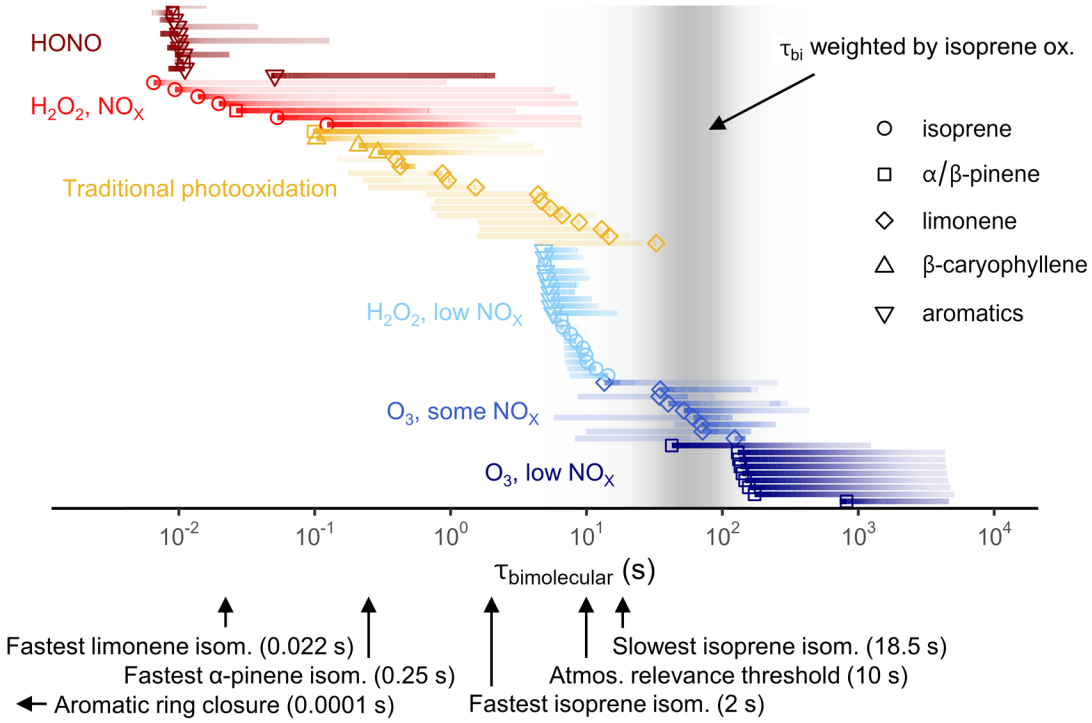

Figure 4: τ_{bi} in chamber experiments and in the atmosphere. The shaded gray region represents the atmospheric distribution of RO_2 bimolecular lifetimes taken from GEOS-Chem, weighted by total isoprene reaction rate. The shading is proportional to the frequency of a given atmospheric τ_{bi}. Modeled chamber experiments are represented by points with tails. Each point represents the τ_{bi} at the start of the experiment while the tail shows the evolution of τ_{bi} over the course of the experiment. The tail transparency is scaled to the percentage of precursor remaining. Point shape and color correspond to precursor identity and experiment category (Table 1), respectively. Lifetimes corresponding to a range of relevant isomerization rates included in the box model are annotated at the bottom of the plot. Values of τ_{uni} are included in parentheses.

Figure 4 demonstrates that experimental τ_{bi} varies over many orders of magnitude. Given this wide range, only a limited number of experiments fall within the global atmospheric lifetime distribution of RO_2 radicals weighted by isoprene oxidation (centered at ~ 60 s and shown in gray; the distribution is similar when weighted by monoterpene oxidation[21]), demonstrating that laboratory conditions usually differ from those found in the atmosphere. However, despite the large overall spread, experiments can clearly be grouped by their oxidation conditions. Experiments featuring high levels of added NO_X fall around $\tau_{bi} < \sim 1$ s, H_2O_2 experiments fall near $\tau_{bi} = 10$ s, ozonolysis with some NO_X fall around $\tau_{bi} = 10 – 100$ s, and low-NO_X ozonolysis falls around $\tau_{bi} > \sim 100$ s. While many "traditional photooxidation" experiments feature τ_{bi} on the order of 1 s, some experiments[30] feature longer τ_{bi} despite high NO_X levels, due to suppression of NO by O_3. The RO_2 bimolecular lifetime also varies within experiments (the "tails" in Fig. 4), often increasing by more than an order of magnitude due to decreasing HO_X and NO_X levels.

While for very long or very short τ_{bi}, this change over time may not substantially affect observed chemistry, shifts across intermediate τ_{bi} may affect the importance of unimolecular reactions as the experiment proceeds.

Comparing the RO_2 bimolecular lifetime to the unimolecular lifetime of a given isomerization reaction indicates whether that reaction will occur. The unimolecular lifetimes corresponding to a selection of isomerization rates used in the model are annotated in Figure 4 (slower isomerization reactions are not shown, as only the relatively fast ones are included in the mechanisms). While these vary by several orders of magnitude, all are shorter than the mean of the atmospheric τ_{bi} distribution, indicating that these reactions will play an important role under most atmospheric conditions. This is consistent with an "atmospherically relevant" threshold of 0.1 s^{-1} (τ_{uni} = 10 s), which has been used to represent a lower bound for the rate at which unimolecular chemistry can proceed as a substantial fraction of RO_2 fate.[7] The majority of low-NO_X experiments involve τ_{bi} near or greater than this threshold, indicating that these chamber experiments included the effects isomerization reactions, even well before the importance of RO_2 isomerization reactions was appreciated. In contrast, higher NO_X experiments feature a shorter τ_{bi} that prevents all but the fastest reactions from occurring.

The wide variability of both experimental τ_{bi} and isomerization rates complicate the relationship between experimental measurements and model SOA parameterizations. Where an isomerization channel is extremely fast (e.g., ring closure reactions in aromatic species) so as to outcompete bimolecular reactions under all conditions, the exclusion of isomerization in the parameterization does not matter, since this reaction will always occur. In contrast, many "atmospherically-relevant" isomerization reactions ($\tau_{uni} \leq 10$ s) occur only under low-NO_X H_2O_2 and ozonolysis conditions, thereby playing a role in the gas-phase chemistry (and ultimately aerosol formation) in these experiments. While the importance of these reactions in such experiments may not perfectly match that of atmospheric conditions,[50] their occurrence in chamber experiments means that rapid isomerization processes are to some extent built into the global model aerosol parameterization for RO_2 + HO_2 conditions. However, chamber experiments are unlikely to perfectly capture the importance of isomerization under most atmospheric conditions. Moreover, under high-NO_X conditions, isomerization is largely quenched, such that little to no isomerization is built into the aerosol parameterization for the high-NO_X conditions.

Changing chemical conditions across yield curves

As mentioned above, aerosol yield curves (aerosol yield vs. mass concentration of organic aerosol) can be used to derive a volatility distribution that is useful for representing SOA in 3D models. An underlying assumption for an aerosol yield curve is that the only modified variable is the mass of organic aerosol into which the gas-phase species partition. However, since the curve is typically made up of measurements across a series of experiments (which typically involve different starting precursor concentrations), variability in chemical conditions across these experiments may affect the resulting aerosol yield curve.

Figure 5 illustrates how chemical conditions can vary across a series of aerosol yield experiments. In this series of experiments, Zhang et al.[30] oxidize limonene under dark ozonolysis conditions, with low but nonzero NO_X. While these experiments were designed to favor the reaction of limonene with ozone, the NO_X present is sufficient to make reaction with NO_3 an important contributor to limonene oxidation. As shown in Figure 5a, this is most pronounced for experiments with low initial precursor concentrations and hence low organic aerosol concentrations (c_{OA}); this is due to variation of the NO_3/O_3 among experiments. Further, at high precursor concentrations (and high c_{OA}), OH generated by the ozonolysis of limonene starts to become an important oxidant, exceeding the capacity of the OH scavenger (5 ppm 2-butanol) to keep [OH] low.

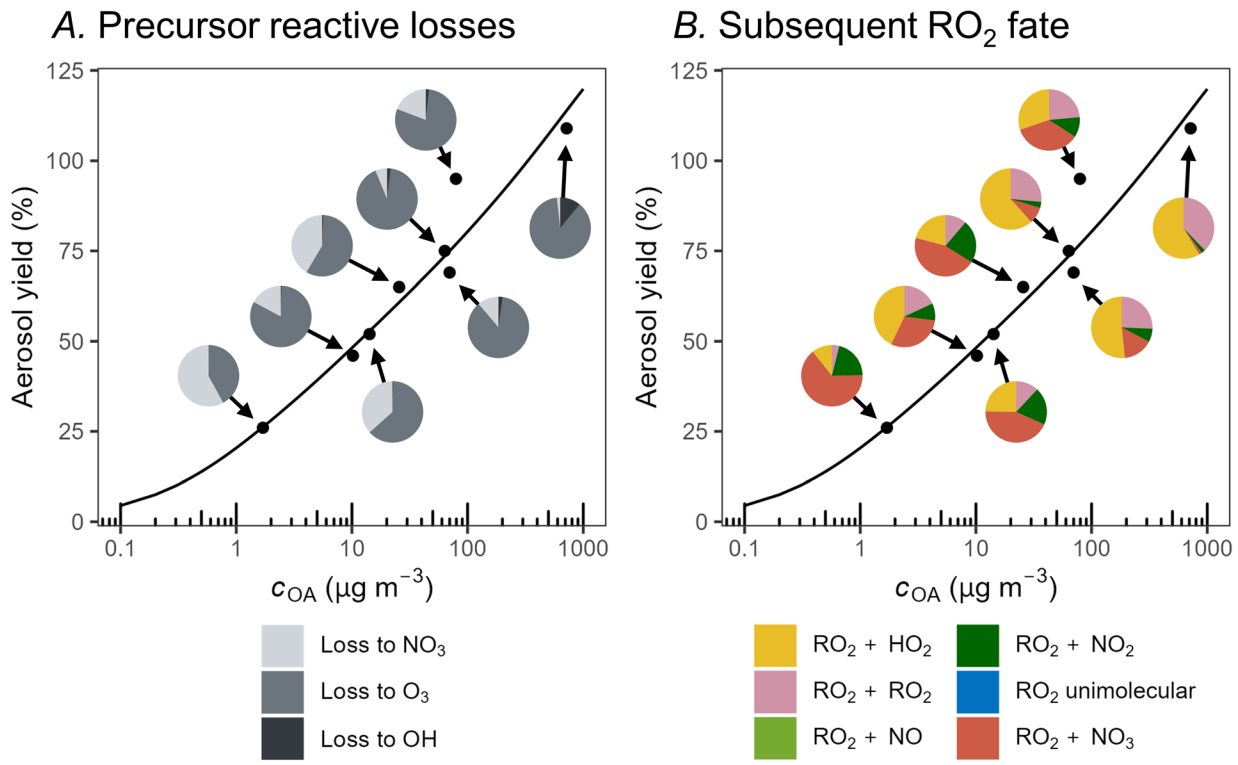

Figure 5: Modeled chemical conditions as a function of measured organic aerosol mass and organic aerosol yield for an example set of experiments. Panel A shows the distribution of precursor reactive loss (integrated over the entire chamber run) for experiments featuring the oxidation of limonene (O_3, some NO_X) from Zhang et al.[30] (expt. 8 – 15). Each experiment is depicted as a pie chart, plotted across the aerosol mass vs aerosol yield space. Panel B shows subsequent RO_2 fate for the same series of experiments plotted in the same way.

Peroxy radical chemistry may also shift as a function of precursor VOC concentration (and therefore c_{OA}). While initial peroxy radical fate is relatively stable across these experiments (see Figure S.5), Figure 5B shows that subsequent RO_2 fate can also shift across a series of experiments. At low precursor concentrations (low c_{OA}), reactions with NO_3 and NO_2 are relatively important, while $RO_2 + RO_2$ reactions become more important at higher precursor concentrations (and higher c_{OA}). While our modeled subsequent chemistry does not include

isomerization reactions that can redistribute RO_2 fate, variations in bimolecular chemistry, due for example to differing total RO_2 concentrations, are likely to persist.

While Fig 5 (Zhang et al.[30]) provides an example of how chemical conditions may shift across an aerosol yield curve, conditions can be more uniform for other experiment types, as shown in Figures S.7 to S.12. For experiments which clearly favor a single oxidant or RO_2 fate (e.g., low-NO_X H_2O_2 experiments), changes in VOC concentration or NO_X background have a smaller impact on modeled chemical conditions. Nonetheless some shifts, such as changes in the prevalence of RO_2 + RO_2 reactions, can appear even under these more extreme conditions (Figure S.8 and S.10).

Implications

This work demonstrates that chemical conditions in an environmental chamber often represent a complex mix of VOC reactive loss pathways and RO_2 fates, making it challenging to assign a single pathway to a given experiment. Conditions often vary over the course of an experiment, and between relatively similar experiments. These changes occur in both the VOC loss pathways and the peroxy radical fate, and are caused by multiple factors. VOC loss pathways can shift as a result of changes not only in oxidant concentration, but also in reactivity, as ozone reactivity and capacity for photolysis changes as the VOC mixture evolves. Peroxy radical fates similarly shift as an experiment proceeds, with NO_2 driving later-generation PAN formation, greater total RO_2 concentrations increasing RO_2 + RO_2 reactions, and decreasing NO and HO_2 leading to increases in the importance of unimolecular reactions (due to increases in τ_{bi}).

Patterns in relative VOC loss pathways and RO_2 fate arise that are correlated with the varied sets of starting oxidation conditions. While chamber experiments using HONO, H_2O_2 (with or without NO_X), and ozone (without NO_X) all feature oxidation dominated by a single oxidant, other types of experiments (traditional photooxidation and "O_3, some NO_X") involve a mixture of oxidants, due to the formation of substantial OH, O_3, and NO_3 concentrations. RO_2 conditions can similarly be grouped by experiment type, with comparable bimolecular lifetimes and fractional RO_2 fate between like experiments; few experimental conditions (low-NO_X H_2O_2, HONO) consistently favor a single RO_2 fate.

The dynamic chemistry observed here may be relevant for the calculation of aerosol yield curves, which represent the basis for aerosol parameterizations. As shown in this work, chemical conditions, including both oxidant and peroxy radical fate, can sometimes vary across a series of SOA experiments from which an aerosol yield curve is derived. Shifts in chemical conditions which vary as a function of precursor concentration (and hence c_{OA}) may skew measured yields, resulting in fitted volatility distributions that do not represent a single chemical condition. The extent to which these changes may affect measured aerosol formation is unclear, as these changes are often subtle, and the specific impact of shifting oxidant or RO_2 fate on SOA formation is often not well understood.

When considering the application of SOA chamber studies to 3D modeling, we find that experimental oxidant and RO_2 conditions for a given experiment do not always match how it is used in a 3D model aerosol parameterization. Most notably, the GEOS-Chem SOA parameterization bases some low-NO_X SOA formation on experiments in which NO_X concentrations are high enough to influence observed chemistry. With more experimental data now available, reevaluating and constraining aerosol parameterizations may represent a valuable avenue for future research. Further, since the atmosphere can involve mixed chemical fates, future work should additionally consider whether the basis for SOA parameterizations should expand beyond experiments targeting single oxidants or RO_2 fates.[21]

Finally, this work highlights the importance of considering RO_2 fates beyond NO and HO_2 for regional and global SOA parameterizations. Despite the limitations of previous SOA experiments, RO_2 isomerization reactions, whose importance for SOA formation was not yet appreciated when these experiments were carried out, proceed under many of the experimental conditions used. Ozonolysis or H_2O_2 experiments with no added NOx feature relatively long bimolecular lifetimes ($\tau_{bi} > \sim 10$ s), allowing for reasonably rapid isomerization ($\tau_{uni} < \sim 10$ s) to occur. Because of this, HO_2-pathway aerosol yields in 3D models implicitly include the effects of some RO_2 isomerization on aerosol yields. Still, chamber experiments rarely fall into the same range of bimolecular lifetimes that occur in the atmosphere, indicating that laboratory peroxy radical conditions generally do not fully match those in the real environment.[21] Ultimately, it is not clear whether this approach to yield parameterizations is sufficient to characterize aerosol formation in the real atmosphere, which may involve slower isomerization processes that do not occur in a lab setting, or isomerization processes that may at times compete with reaction with NO.

This study seeks to explore unmeasured chamber conditions used in key historical SOA experiments, and in doing so, identifies patterns that may be useful both for designing laboratory experiments and for implementing parameterizations of laboratory chemistry into models. Future experimental work should consider the role of changing chemical fate with respect to first- and later-generation compounds, and the influence of changing starting conditions across sets of aerosol yield experiments (Figure 5). Alternative experimental designs, such as the use of steady-state continuous flow chamber experiments, may help mitigate the challenges associated with conditions that change over the course of an experiment. Future SOA model schemes must at least consider the uncertainties in experimental chemical conditions, if not explore the development of wholly new frameworks to translate experimental yield measurements to the modeling sphere.

Data availability

Data for this article, including all figure data, Matlab code, and model input conditions are available on the Kroll Group publication website at http://krollgroup.mit.edu/publications.html.

Author contributions

MBG performed all box modeling, analyzed the data, and wrote the paper. HSK assisted in framing the project, provided GEOS-Chem output, and shared code relevant to RO_2 fate analysis. CLH aided in project design and manuscript preparation. JHK aided in project conceptualization, project design, data interpretation, and manuscript preparation.

Acknowledgements

The authors thank Sally Ng for providing data from two publications that was not previously publicly accessible.[26,27] JHK would like to express his deep gratitude to John Seinfeld for introducing him to SOA and chamber studies, and more importantly for all the mentorship and support over the years.

Financial Support

This work was supported by Department of Energy grant DE-SC0022017 and National Science Foundation grant AGS-2129835. MBG was supported by the Training Grant in Environmental Toxicology (MIT Center for Environmental Health Sciences, NIEHS Grant # T32-ES007020 and Grant # P30-ES002109), the MathWorks Engineering Fellowship Fund, and the Harvard University Center for the Environment (HUCE) Environmental Fellows Program. HSK was supported by National Science Foundation grant AGS-PRF-2137238.

References

(1) Zhang, Q.; Jimenez, J. L.; Canagaratna, M. R.; Allan, J. D.; Coe, H.; Ulbrich, I.; Alfarra, M. R.; Takami, A.; Middlebrook, A. M.; Sun, Y. L.; Dzepina, K.; Dunlea, E.; Docherty, K.; DeCarlo, P. F.; Salcedo, D.; Onasch, T.; Jayne, J. T.; Miyoshi, T.; Shimono, A.; Hatakeyama, S.; Takegawa, N.; Kondo, Y.; Schneider, J.; Drewnick, F.; Borrmann, S.; Weimer, S.; Demerjian, K.; Williams, P.; Bower, K.; Bahreini, R.; Cottrell, L.; Griffin, R. J.; Rautiainen, J.; Sun, J. Y.; Zhang, Y. M.; Worsnop, D. R. Ubiquity and Dominance of Oxygenated Species in Organic Aerosols in Anthropogenically-Influenced Northern Hemisphere Midlatitudes. *Geophys. Res. Lett.* **2007**, *34* (13). https://doi.org/10.1029/2007GL029979.

(2) Jimenez, J. L.; Canagaratna, M. R.; Donahue, N. M.; Prevot, A. S. H.; Zhang, Q.; Kroll, J. H.; DeCarlo, P. F.; Allan, J. D.; Coe, H.; Ng, N. L.; Aiken, A. C.; Docherty, K. S.; Ulbrich, I. M.; Grieshop, A. P.; Robinson, A. L.; Duplissy, J.; Smith, J. D.; Wilson, K. R.; Lanz, V. A.; Hueglin, C.; Sun, Y. L.; Tian, J.; Laaksonen, A.; Raatikainen, T.; Rautiainen, J.; Vaattovaara, P.; Ehn, M.; Kulmala, M.; Tomlinson, J. M.; Collins, D. R.; Cubison, M. J.; E.; Dunlea, J.; Huffman, J. A.; Onasch, T. B.; Alfarra, M. R.; Williams, P. I.; Bower, K.; Kondo, Y.; Schneider, J.; Drewnick, F.; Borrmann, S.; Weimer, S.; Demerjian, K.; Salcedo, D.; Cottrell, L.; Griffin, R.; Takami, A.; Miyoshi, T.; Hatakeyama, S.; Shimono, A.; Sun, J. Y.; Zhang, Y. M.; Dzepina, K.; Kimmel, J. R.; Sueper, D.; Jayne, J. T.; Herndon, S. C.; Trimborn, A. M.; Williams, L. R.; Wood, E. C.; Middlebrook, A. M.; Kolb, C. E.; Baltensperger, U.; Worsnop, D. R. Evolution of Organic Aerosols in the Atmosphere. *Science* **2009**, *326* (5959), 1525–1529. https://doi.org/10.1126/science.1180353.

(3) Tsigaridis, K.; Daskalakis, N.; Kanakidou, M.; Adams, P. J.; Artaxo, P.; Bahadur, R.; Balkanski, Y.; Bauer, S. E.; Bellouin, N.; Benedetti, A.; Bergman, T.; Berntsen, T. K.; Beukes, J. P.; Bian, H.; Carslaw, K. S.; Chin, M.; Curci, G.; Diehl, T.; Easter, R. C.; Ghan, S. J.; Gong, S. L.; Hodzic, A.; Hoyle, C. R.; Iversen, T.; Jathar, S.; Jimenez, J. L.; Kaiser, J. W.; Kirkevåg, A.; Koch, D.; Kokkola, H.; Lee, Y. H.; Lin, G.; Liu, X.; Luo, G.; Ma, X.; Mann, G. W.; Mihalopoulos, N.; Morcrette, J.-J.; Müller, J.-F.; Myhre, G.; Myriokefalitakis, S.; Ng, N. L.; O'Donnell, D.; Penner, J. E.; Pozzoli, L.; Pringle, K. J.; Russell, L. M.; Schulz, M.; Sciare, J.; Seland, Ø.; Shindell, D. T.; Sillman, S.; Skeie, R. B.; Spracklen, D.; Stavrakou, T.; Steenrod, S. D.; Takemura, T.; Tiitta, P.; Tilmes, S.; Tost, H.; van Noije, T.; van Zyl, P. G.; von Salzen, K.; Yu, F.; Wang, Z.; Zaveri, R. A.; Zhang, H.; Zhang, K.; Zhang, Q.; Zhang, X. The AeroCom Evaluation and Intercomparison of Organic Aerosol in Global Models. *Atmospheric Chem. Phys.* **2014**, *14* (19), 10845–10895. https://doi.org/10.5194/acp-14-10845-2014.

(4) Pai, S. J.; Heald, C. L.; Pierce, J. R.; Farina, S. C.; Marais, E. A.; Jimenez, J. L.; Campuzano-Jost, P.; Nault, B. A.; Middlebrook, A. M.; Coe, H.; Shilling, J. E.; Bahreini, R.; Dingle, J. H.; Vu, K. An Evaluation of Global Organic Aerosol Schemes Using Airborne Observations. *Atmospheric Chem. Phys.* **2020**, *20* (5), 2637–2665. https://doi.org/10.5194/acp-20-2637-2020.

(5) Kroll, J. H.; Seinfeld, J. H. Chemistry of Secondary Organic Aerosol: Formation and Evolution of Low-Volatility Organics in the Atmosphere. *Atmos. Environ.* **2008**, *42* (16), 3593–3624. https://doi.org/10.1016/j.atmosenv.2008.01.003.

(6) Vaughan, S.; Canosa-Mas, C. E.; Pfrang, C.; Shallcross, D. E.; Watson, L.; Wayne, R. P. Kinetic Studies of Reactions of the Nitrate Radical (NO3) with Peroxy Radicals (RO2): An Indirect Source of OH at Night? *Phys. Chem. Chem. Phys.* **2006**, *8* (32), 3749. https://doi.org/10.1039/b605569a.

(7) Crounse, J. D.; Nielsen, L. B.; Jørgensen, S.; Kjaergaard, H. G.; Wennberg, P. O. Autoxidation of Organic Compounds in the Atmosphere. *J. Phys. Chem. Lett.* **2013**, *4* (20), 3513–3520. https://doi.org/10.1021/jz4019207.

(8) Ehn, M.; Thornton, J. A.; Kleist, E.; Sipilä, M.; Junninen, H.; Pullinen, I.; Springer, M.; Rubach, F.; Tillmann, R.; Lee, B.; Lopez-Hilfiker, F.; Andres, S.; Acir, I.-H.; Rissanen, M.; Jokinen, T.; Schobesberger, S.; Kangasluoma, J.; Kontkanen, J.; Nieminen, T.; Kurtén, T.; Nielsen, L. B.; Jørgensen, S.; Kjaergaard, H. G.; Canagaratna, M.; Maso, M. D.; Berndt, T.; Petäjä, T.; Wahner, A.; Kerminen, V.-M.; Kulmala, M.; Worsnop, D. R.; Wildt, J.; Mentel, T. F. A Large Source of Low-Volatility Secondary Organic Aerosol. *Nature* **2014**, *506* (7489), 476–479. https://doi.org/10.1038/nature13032.

(9) Vereecken, L.; Nozière, B. H Migration in Peroxy Radicals under Atmospheric Conditions. *Atmospheric Chem. Phys.* **2020**, *20* (12), 7429–7458. https://doi.org/10.5194/acp-20-7429-2020.

(10) Berndt, T.; Scholz, W.; Mentler, B.; Fischer, L.; Herrmann, H.; Kulmala, M.; Hansel, A. Accretion Product Formation from Self- and Cross-Reactions of RO2 Radicals in the Atmosphere. *Angew. Chem. Int. Ed.* **2018**, *57* (14), 3820–3824. https://doi.org/10.1002/anie.201710989.

(11) Berndt, T.; Chen, J.; Kj, E. R.; Hoffmann, E. H.; Herrmann, H.; Crounse, J. D.; Wennberg, P. O.; Kjaergaard, H. G. Hydrotrioxide (ROOOH) Formation in the Atmosphere. **2022**, 5.

(12) Farina, S. C.; Adams, P. J.; Pandis, S. N. Modeling Global Secondary Organic Aerosol Formation and Processing with the Volatility Basis Set: Implications for Anthropogenic Secondary Organic Aerosol. *J. Geophys. Res. Atmospheres* **2010**, *115* (D9). https://doi.org/10.1029/2009JD013046.

(13) Pankow, J. F. An Absorption Model of the Gas/Aerosol Partitioning Involved in the Formation of Secondary Organic Aerosol. *Atmos. Environ.* **1994**, *28* (2), 189–193. https://doi.org/10.1016/1352-2310(94)90094-9.

(14) Odum, J. R.; Hoffmann, T.; Bowman, F.; Collins, D.; Flagan, R. C.; Seinfeld, J. H. Gas/Particle Partitioning and Secondary Organic Aerosol Yields. *Environ. Sci. Technol.* **1996**, *30* (8), 2580–2585. https://doi.org/10.1021/es950943+.

(15) Donahue, N. M.; Robinson, A. L.; Stanier, C. O.; Pandis, S. N. Coupled Partitioning, Dilution, and Chemical Aging of Semivolatile Organics. *Environ. Sci. Technol.* **2006**, *40* (8), 2635–2643. https://doi.org/10.1021/es052297c.

(16) Presto, A. A.; Donahue, N. M. Investigation of α-Pinene + Ozone Secondary Organic Aerosol Formation at Low Total Aerosol Mass. *Environ. Sci. Technol.* **2006**, *40* (11), 3536–3543. https://doi.org/10.1021/es052203z.

(17) Henze, D. K.; Seinfeld, J. H.; Ng, N. L.; Kroll, J. H.; Fu, T.-M.; Jacob, D. J.; Heald, C. L. Global Modeling of Secondary Organic Aerosol Formation from Aromatic Hydrocarbons: High- vs. Low-Yield Pathways. *Atmospheric Chem. Phys.* **2008**, *8* (9), 2405–2420. https://doi.org/10.5194/acp-8-2405-2008.

(18) Pye, H. O. T.; Chan, A. W. H.; Barkley, M. P.; Seinfeld, J. H. Global Modeling of Organic Aerosol: The Importance of Reactive Nitrogen (NO_X and NO_3). *Atmospheric Chem. Phys.* **2010**, *10* (22), 11261–11276. https://doi.org/10.5194/acp-10-11261-2010.

(19) Porter, W. C.; Jimenez, J. L.; Barsanti, K. C. Quantifying Atmospheric Parameter Ranges for Ambient Secondary Organic Aerosol Formation. *ACS Earth Space Chem.* **2021**, *5* (9), 2380–2397. https://doi.org/10.1021/acsearthspacechem.1c00090.

(20) Krechmer, J. E.; Day, D. A.; Jimenez, J. L. Always Lost but Never Forgotten: Gas-Phase Wall Losses Are Important in All Teflon Environmental Chambers. *Environ. Sci. Technol.* **2020**, *54* (20), 12890–12897. https://doi.org/10.1021/acs.est.0c03381.

(21) Kenagy, H. S.; Heald, C. L.; Tahsini, N.; Goss, M. B.; Kroll, J. H. Can We Achieve Atmospheric Chemical Environments in the Laboratory? An Integrated Model-Measurement Approach to Chamber SOA Studies. *Sci. Adv.* **2024**, *10* (37), eado1482. https://doi.org/10.1126/sciadv.ado1482.

(22) Zhang, X.; Cappa, C. D.; Jathar, S. H.; McVay, R. C.; Ensberg, J. J.; Kleeman, M. J.; Seinfeld, J. H. Influence of Vapor Wall Loss in Laboratory Chambers on Yields of Secondary Organic Aerosol. *Proc. Natl. Acad. Sci.* **2014**, *111* (16), 5802–5807. https://doi.org/10.1073/pnas.1404727111.

(23) Fisher, J. A.; Jacob, D. J.; Travis, K. R.; Kim, P. S.; Marais, E. A.; Chan Miller, C.; Yu, K.; Zhu, L.; Yantosca, R. M.; Sulprizio, M. P.; Mao, J.; Wennberg, P. O.; Crounse, J. D.; Teng,

A. P.; Nguyen, T. B.; St. Clair, J. M.; Cohen, R. C.; Romer, P.; Nault, B. A.; Wooldridge, P. J.; Jimenez, J. L.; Campuzano-Jost, P.; Day, D. A.; Hu, W.; Shepson, P. B.; Xiong, F.; Blake, D. R.; Goldstein, A. H.; Misztal, P. K.; Hanisco, T. F.; Wolfe, G. M.; Ryerson, T. B.; Wisthaler, A.; Mikoviny, T. Organic Nitrate Chemistry and Its Implications for Nitrogen Budgets in an Isoprene- and Monoterpene-Rich Atmosphere: Constraints from Aircraft (SEAC^{4}RS) and Ground-Based (SOAS) Observations in the Southeast US. *Atmospheric Chem. Phys.* **2016**, *16* (9), 5969–5991. https://doi.org/10.5194/acp-16-5969-2016.

(24) Marais, E. A.; Jacob, D. J.; Jimenez, J. L.; Campuzano-Jost, P.; Day, D. A.; Hu, W.; Krechmer, J.; Zhu, L.; Kim, P. S.; Miller, C. C.; Fisher, J. A.; Travis, K.; Yu, K.; Hanisco, T. F.; Wolfe, G. M.; Arkinson, H. L.; Pye, H. O. T.; Froyd, K. D.; Liao, J.; McNeill, V. F. Aqueous-Phase Mechanism for Secondary Organic Aerosol Formation from Isoprene: Application to the Southeast United States and Co-Benefit of SO_2 Emission Controls. *Atmospheric Chem. Phys.* **2016**, *16* (3), 1603–1618. https://doi.org/10.5194/acp-16-1603-2016.

(25) Wennberg, P. O. Let's Abandon the "High NO_X" and "Low NO_X" Terminology. *ACS EST Air* **2024**, *1* (1), 3–4. https://doi.org/10.1021/acsestair.3c00055.

(26) Ng, N. L.; Chhabra, P. S.; Chan, A. W. H.; Surratt, J. D.; Kroll, J. H.; Kwan, A. J.; McCabe, D. C.; Wennberg, P. O.; Sorooshian, A.; Murphy, S. M.; Dalleska, N. F.; Flagan, R. C.; Seinfeld, J. H. Effect of NOx Level on Secondary Organic Aerosol (SOA) Formation from the Photooxidation of Terpenes. *Atmos Chem Phys* **2007**, 16.

(27) Ng, N. L.; Kroll, J. H.; Chan, A. W. H.; Chhabra, P. S.; Flagan, R. C.; Seinfeld, J. H. Secondary Organic Aerosol Formation from *m*-Xylene, Toluene, and Benzene. *Atmospheric Chem. Phys.* **2007**, *7* (14), 3909–3922. https://doi.org/10.5194/acp-7-3909-2007.

(28) Kroll, J. H.; Ng, N. L.; Murphy, S. M.; Flagan, R. C.; Seinfeld, J. H. Secondary Organic Aerosol Formation from Isoprene Photooxidation. *Environ. Sci. Technol.* **2006**, *40* (6), 1869–1877. https://doi.org/10.1021/es0524301.

(29) Griffin, R. J.; Cocker, D. R.; Flagan, R. C.; Seinfeld, J. H. Organic Aerosol Formation from the Oxidation of Biogenic Hydrocarbons. *J. Geophys. Res. Atmospheres* **1999**, *104* (D3), 3555–3567. https://doi.org/10.1029/1998JD100049.

(30) Zhang, J.; Huff Hartz, K. E.; Pandis, S. N.; Donahue, N. M. Secondary Organic Aerosol Formation from Limonene Ozonolysis: Homogeneous and Heterogeneous Influences as a Function of NO_X. *J. Phys. Chem. A* **2006**, *110* (38), 11053–11063. https://doi.org/10.1021/jp062836f.

(31) Shilling, J. E.; Chen, Q.; King, S. M.; Rosenoern, T.; Kroll, J. H.; Worsnop, D. R.; McKinney, K. A.; Martin, S. T. Particle Mass Yield in Secondary Organic Aerosol Formed by the Dark Ozonolysis of α-Pinene. *Atmos Chem Phys* **2008**, 16.

(32) Wolfe, G. M.; Marvin, M. R.; Roberts, S. J.; Travis, K. R.; Liao, J. The Framework for 0-D Atmospheric Modeling (F0AM) v3.1. *Geosci. Model Dev.* **2016**, *9* (9), 3309–3319. https://doi.org/10.5194/gmd-9-3309-2016.

(33) Jenkin, M. E.; Saunders, S. M.; Pilling, M. J. The Tropospheric Degradation of Volatile Organic Compounds: A Protocol for Mechanism Development. *Atmos. Environ.* **1997**, *31* (1), 81–104. https://doi.org/10.1016/S1352-2310(96)00105-7.

(34) Jenkin, M. E.; Saunders, S. M.; Wagner, V.; Pilling, M. J. Protocol for the Development of the Master Chemical Mechanism, MCM v3 (Part B): Tropospheric Degradation of Aromatic Volatile Organic Compounds. *Atmospheric Chem. Phys.* **2003**, *3* (1), 181–193. https://doi.org/10.5194/acp-3-181-2003.

(35) Jenkin, M. E.; Wyche, K. P.; Evans, C. J.; Carr, T.; Monks, P. S.; Alfarra, M. R.; Barley, M. H.; McFiggans, G. B.; Young, J. C.; Rickard, A. R. Development and Chamber Evaluation of the MCM v3.2 Degradation Scheme for β-Caryophyllene. *Atmospheric Chem. Phys.* **2012**, *12* (11), 5275–5308. https://doi.org/10.5194/acp-12-5275-2012.

(36) Jenkin, M. E.; Young, J. C.; Rickard, A. R. The MCM v3.3.1 Degradation Scheme for Isoprene. *Atmospheric Chem. Phys. Katlenburg-Lindau* **2015**, *15* (20), 11433–11459. http://dx.doi.org/10.5194/acp-15-11433-2015.

(37) Bloss, C.; Wagner, V.; Jenkin, M. E.; Volkamer, R.; Bloss, W. J.; Lee, J. D.; Heard, D. E.; Wirtz, K.; Martin-Reviejo, M.; Rea, G.; Wenger, J. C.; Pilling, M. J. Development of a Detailed Chemical Mechanism (MCMv3.1) for the Atmospheric Oxidation of Aromatic Hydrocarbons. *Atmospheric Chem. Phys.* **2005**, *5* (3), 641–664. https://doi.org/10.5194/acp-5-641-2005.

(38) Ng, N. L.; Kwan, A. J.; Surratt, J. D.; Chan, A. W. H.; Chhabra, P. S.; Sorooshian, A.; Pye, H. O. T.; Crounse, J. D.; Wennberg, P. O.; Flagan, R. C.; Seinfeld, J. H. Secondary Organic Aerosol (SOA) Formation from Reaction of Isoprene with Nitrate Radicals (NO_3). *Atmospheric Chem. Phys.* **2008**, *8* (14), 4117–4140. https://doi.org/10.5194/acp-8-4117-2008.

(39) Iyer, S.; Rissanen, M. P.; Valiev, R.; Barua, S.; Krechmer, J. E.; Thornton, J.; Ehn, M.; Kurtén, T. Molecular Mechanism for Rapid Autoxidation in α-Pinene Ozonolysis. *Nat. Commun.* **2021**, *12* (1), 878. https://doi.org/10.1038/s41467-021-21172-w.

(40) Møller, K. H.; Otkjær, R. V.; Chen, J.; Kjaergaard, H. G. Double Bonds Are Key to Fast Unimolecular Reactivity in First-Generation Monoterpene Hydroxy Peroxy Radicals. *J. Phys. Chem. A* **2020**, *124* (14), 2885–2896. https://doi.org/10.1021/acs.jpca.0c01079.

(41) Pang, J. Y. S.; Novelli, A.; Kaminski, M.; Acir, I.-H.; Bohn, B.; Carlsson, P. T. M.; Cho, C.; Dorn, H.-P.; Hofzumahaus, A.; Li, X.; Lutz, A.; Nehr, S.; Reimer, D.; Rohrer, F.; Tillmann, R.; Wegener, R.; Kiendler-Scharr, A.; Wahner, A.; Fuchs, H. Investigation of the Limonene Photooxidation by OH at Different NO Concentrations in the Atmospheric Simulation Chamber SAPHIR (Simulation of Atmospheric PHotochemistry In a Large Reaction Chamber). *Atmospheric Chem. Phys.* **2022**, *22* (13), 8497–8527. https://doi.org/10.5194/acp-22-8497-2022.

(42) Vereecken, L. Reaction Mechanisms for the Atmospheric Oxidation of Monocyclic Aromatic Compounds. In *Advances in Atmospheric Chemistry*; Advances in Atmospheric Chemistry; WORLD SCIENTIFIC, 2018; Vol. Volume 2, pp 377–527. https://doi.org/10.1142/9789813271838_0006.

(43) Vereecken, L.; Vu, G.; Wahner, A.; Kiendler-Scharr, A.; Nguyen, H. M. T. A Structure Activity Relationship for Ring Closure Reactions in Unsaturated Alkylperoxy Radicals. *Phys. Chem. Chem. Phys.* **2021**, *23* (31), 16564–16576. https://doi.org/10.1039/D1CP02758A.

(44) Xu, L.; Møller, K. H.; Crounse, J. D.; Otkjær, R. V.; Kjaergaard, H. G.; Wennberg, P. O. Unimolecular Reactions of Peroxy Radicals Formed in the Oxidation of α-Pinene and β-Pinene by Hydroxyl Radicals. *J. Phys. Chem. A* **2019**, *123* (8), 1661–1674. https://doi.org/10.1021/acs.jpca.8b11726.

(45) Cocker, D. R.; Flagan, R. C.; Seinfeld, J. H. State-of-the-Art Chamber Facility for Studying Atmospheric Aerosol Chemistry. *Environ. Sci. Technol.* **2001**, *35* (12), 2594–2601. https://doi.org/10.1021/es0019169.

(46) Presto, A. A.; Huff Hartz, K. E.; Donahue, N. M. Secondary Organic Aerosol Production from Terpene Ozonolysis. 1. Effect of UV Radiation. *Environ. Sci. Technol.* **2005**, *39* (18), 7036–7045. https://doi.org/10.1021/es050174m.

(47) da Silva, G.; Graham, C.; Wang, Z.-F. Unimolecular β-Hydroxyperoxy Radical Decomposition with OH Recycling in the Photochemical Oxidation of Isoprene. *Environ. Sci. Technol.* **2010**, *44* (1), 250–256. https://doi.org/10.1021/es900924d.

(48) Crounse, J. D.; Paulot, F.; Kjaergaard, H. G.; Wennberg, P. O. Peroxy Radical Isomerization in the Oxidation of Isoprene. *Phys. Chem. Chem. Phys.* **2011**, *13* (30), 13607–13613. https://doi.org/10.1039/C1CP21330J.

(49) Teng, A. P.; Crounse, J. D.; Wennberg, P. O. Isoprene Peroxy Radical Dynamics. *J. Am. Chem. Soc.* **2017**, *139* (15), 5367–5377. https://doi.org/10.1021/jacs.6b12838.

(50) D'Ambro, E. L.; Møller, K. H.; Lopez-Hilfiker, F. D.; Schobesberger, S.; Liu, J.; Shilling, J. E.; Lee, B. H.; Kjaergaard, H. G.; Thornton, J. A. Isomerization of Second-Generation Isoprene Peroxy Radicals: Epoxide Formation and Implications for Secondary Organic Aerosol Yields. *Environ. Sci. Technol.* **2017**, *51* (9), 4978–4987. https://doi.org/10.1021/acs.est.7b00460.

(51) Pathak, R. K.; Stanier, C. O.; Donahue, N. M.; Pandis, S. N. Ozonolysis of α-Pinene at Atmospherically Relevant Concentrations: Temperature Dependence of Aerosol Mass Fractions (Yields). *J. Geophys. Res. Atmospheres* **2007**, *112* (D3). https://doi.org/10.1029/2006JD007436.

(52) Fry, J. L.; Draper, D. C.; Barsanti, K. C.; Smith, J. N.; Ortega, J.; Winkler, P. M.; Lawler, M. J.; Brown, S. S.; Edwards, P. M.; Cohen, R. C.; Lee, L. Secondary Organic Aerosol Formation and Organic Nitrate Yield from NO3 Oxidation of Biogenic Hydrocarbons. *Environ. Sci. Technol.* **2014**, *48* (20), 11944–11953. https://doi.org/10.1021/es502204x.